Supporting Information

Metal self-assembly mimosine peptides with enhanced antimicrobial activity: towards a new generation of multitasking chelating agents.

Joanna Izabela Lachowicz,[*a] Gabriele Dalla Torre,[b,c] Rosita Cappai,[d] Enrico Randaccio,[e] Valeria M. Nurchi[d], Remigiusz Bachor,[e] Zbigniew Szewczuk,[e] Lukasz Jaremko,[f] Mariusz Jaremko,[f] Maria Barbara Pisano,[g] Sofia Cosentino,[g] Germano Orrù,[h] Antonella Ibba,[h] Joni Mujika,[b] and Xabier Lopez[b,*].

[a]*Department of Medical Sciences and Public Health, University of Cagliari, Cittadella Universitaria, 09042 Monserrato, Italy*

[b]*Kimika Fakultatea, Euskal Herriko Unibertsitatea UPV/EHU, Donostia International Physics Center (DIPC), P.K. 1072, Donostia, Euskadi, 20080 San Sebastian, Spain*

[c]*UCIBIO/REQUIMTE, Departamento de Química e Bioquímica, Faculdade de Ciências, Universidade do Porto, Rua do Campo Alegre, s/n, 4169-007 Porto, Portugal.*

[d]*Department of Life Sciences, University of Cagliari, Cittadella Universitaria, 09042 Monserrato, Italy*

[e]*Faculty of Chemistry, University of Wrocław, F. Joliot-Curie 14, 50-383 Wrocław, Poland*

[f]*Division of Biological and Environmental Sciences and Engineering, King Abdullah University of Science and Technology (KAUST), 23955, Thuwal, Saudi Arabia*

[g]*Department of Medical Sciences and Public Health, University of Cagliari, Cittadella Universitaria, 09042 Monserrato, Italy*

[h]*Department of Surgical Sciences, University of Cagliari, Cittadella Universitaria, 09042 Monserrato, Italy*

***Corresponding authors**: Joanna Izabela Lachowicz: lachowicz@unica.it; Xabier Lopez: xabier.lopez@ehu.es*

List of Tables and Figures:

Table S7. 1H and 13C chemical shifts assigned for the Peptide5 H-Mim-Gly-Pro-Gly-Mim-Gly-OH [ppm].

Table S8. 1:3 Fe(III)-DFP crystallographic data compared with DFT optimized geometries of metal coordination core. Optimizations carried out at the B3LYP-D3(BJ)/6-31++(g,d) IEFPCM level of theory. A, B and C distinguish different MIM amino acids, while p (para) and m (meta) is the oxygen (carbonyl and hydroxyl) position respect to the nitrogen in the pyridinone ring.

Table S9. 1:2 Cu(II)-DFP crystallographic data compared with DFT optimized geometries of metal coordination core. Optimizations carried out at the B3LYP-D3(BJ)/6-31++(g,d) IEFPCM level of theory. A, B and C distinguish different MIM amino acids, while p (para) and m (meta) is the oxygen (carbonyl and hydroxyl) position respect to the nitrogen in the pyridinone ring.

Table S10. 1:2 Cu(II)-DFP crystallographic data compared with 2:2 Cu(II)-MIM and 2:2 Cu(II)-P2 DFT optimized geometries of metal coordination core. Optimizations carried out at the B3LYP-D3(BJ)/6-31++(g,d) IEFPCM level of theory. A and B distinguish ligand binding sites in different ligands, while p (para) and m (meta) is the oxygen (carbonyl and hydroxyl) position respect to the nitrogen in the pyridinone ring.

Table S11. 1:1 Fe(III)-peptide DFT optimized geometries data of metal coordination core. Optimizations carried out at the B3LYP-D3(BJ)/6-31++(g,d) IEFPCM level of theory. A, B and C distinguish different MIM amino acids in the peptide, while p (para) and m (meta) is the oxygen (carbonyl and hydroxyl) position respect to the nitrogen in the pyridinone ring. W refers to water molecule.

Table S12. 1:1 Cu(II)-peptide DFT optimized geometries data of metal coordination core. Optimizations carried out at the B3LYP-D3(BJ)/6-31++(g,d) IEFPCM level of theory. A and B distinguish different MIM amino acids in the peptide, while p (para) and m (meta) is the oxygen (carbonyl or hydroxyl) position respect to the nitrogen in the pyridinone ring. W refers to water molecule.

Table S13. 2:2 Cu(II)-peptide DFT optimized geometries data of metal coordination core. Optimizations carried out at the B3LYP-D3(BJ)/6-31++(g,d) IEFPCM level of theory. A1 and B1 distinguish different MIM amino acids in the first peptide in the dimer complex and A2 and B2 distinguish MIM amino acids in the second peptide in the dimer complex, while p (para) and m (meta) is the oxygen (carbonyl or hydroxyl) position respect to the nitrogen in the pyridinone ring.

Table S14. Antimicrobial screening of mimosine derived peptides evaluated using by the agar plate disk diffusion method.

Table S15. Minimum inhibitory concentration (MIC) and minimum bactericidal concentration (MBC) of the mimosine-peptides (μg/mL).

Table S16. Minimum inhibitory concentration (MIC) and minimum bactericidal concentration (MBC) of the mimosine-peptides iron complexes (μg/mL).

Table S17. MIC activity of Peptide 6 with and without iron.

Table S18. Biofilm inhibition activity of Peptide 6 with and without iron.

Figure S7. Graphical representation of biofilm inhibition activity of Peptide 6 with and without iron (Table S16).

Figure S8. Computed binding energies in solution (ΔG_{comp}, in kcal/mol) versus experimental stability constants (logβ) of 1:1, 1:2 and 1:3 Fe(III):Ligand complexes and 1:1 1:2 Cu(II):Ligand complexes, where Ligand can be either DFP or MIM. The correlation coefficient (r) is 0.9873.

Figure S9. ESI-MS spectrum of peptide 1 complex with Fe(III) ions.

Figure S9a. Enlarged fragment of the ESI-MS spectrum of $[Fe(P1)H_{-1}]^+$ complex. Inlet presents the generated isotopic distribution for the $C_{26}H_{34}FeN_6O_8$ ion.

Figure S10. ESI-MS spectrum of peptide 1 complex with Cu(II) ions.

Figure S10a. ESI-MS spectrum of $[Cu(P1)H_{-1}]^+$ complex. Inlet presents the generated isotopic distribution for the $C_{26}H_{34}CuN_6O_8$ ion.

Figure S11. TDDFT spectra of Fe(DFP), using the WB97XD functional [D. Chai and M. Head-Gordon, "Long-range corrected hybrid density functionals with damped atom-atom dispersion corrections," Phys. Chem. Chem. Phys., 10 (2008) 6615-20. DOI: 10.1039/B810189B] and the SMD implicit solvation model [A. V. Marenich, C. J. Cramer, and D. G. Truhlar, "Universal solvation model based on solute electron density and a continuum model of the solvent defined by the bulk dielectric constant and atomic surface tensions," J. Phys. Chem. B, 113 (2009) 6378-96. DOI: 10.1021/jp810292n] with the addition of explicit second-shell water molecules.

Figure S12. TDDFT spectra of $Fe(DFP)_2$, using the WB97XD functional [D. Chai and M. Head-Gordon, "Long-range corrected hybrid density functionals with damped atom-atom dispersion corrections," Phys. Chem. Chem. Phys., 10 (2008) 6615-20. DOI: 10.1039/B810189B] and the SMD implicit solvation model [A. V. Marenich, C. J. Cramer, and D. G. Truhlar, "Universal solvation model based on solute electron density and a continuum model of the solvent defined by

the bulk dielectric constant and atomic surface tensions," J. Phys. Chem. B, 113 (2009) 6378-96. DOI: 10.1021/jp810292n].

Figure S13. TDDFT spectra of $Fe(DFP)_3$, using the WB97XD functional [D. Chai and M. Head-Gordon, "Long-range corrected hybrid density functionals with damped atom-atom dispersion corrections," Phys. Chem. Chem. Phys., 10 (2008) 6615-20. DOI: 10.1039/B810189B] and the SMD implicit solvation model [A. V. Marenich, C. J. Cramer, and D. G. Truhlar, "Universal solvation model based on solute electron density and a continuum model of the solvent defined by the bulk dielectric constant and atomic surface tensions," J. Phys. Chem. B, 113 (2009) 6378-96. DOI: 10.1021/jp810292n].

Figure S14. TDDFT spectra using the WB97XD/6-31G(d) functional [D. Chai and M. Head-Gordon, "Long-range corrected hybrid density functionals with damped atom-atom dispersion corrections," Phys. Chem. Chem. Phys., 10 (2008) 6615-20. DOI: 10.1039/B810189B] and the SMD implicit solvation model [A. V. Marenich, C. J. Cramer, and D. G. Truhlar, "Universal solvation model based on solute electron density and a continuum model of the solvent defined by the bulk dielectric constant and atomic surface tensions," J. Phys. Chem. B, 113 (2009) 6378-96. DOI: 10.1021/jp810292n], for the different peptides (peptides 1 to 6) bound to Fe(III), compared to the experimental and theoretical data for Fe(DFP), $Fe(DFP)_2$ and $Fe(DFP)_3$

Figure S15. TDDFT spectra using the WB97XD/6-311G(d,p) functional [D. Chai and M. Head-Gordon, "Long-range corrected hybrid density functionals with damped atom-atom dispersion corrections," Phys. Chem. Chem. Phys., 10 (2008) 6615-20. DOI: 10.1039/B810189B] and the SMD implicit solvation model [A. V. Marenich, C. J. Cramer, and D. G. Truhlar, "Universal solvation model based on solute electron density and a continuum model of the solvent defined by the bulk dielectric constant and atomic surface tensions," J. Phys. Chem. B, 113 (2009) 6378-96. DOI: 10.1021/jp810292n], for the different peptides (peptides 1 to 6) bound to Fe(III), compared to the experimental and theoretical data for Fe(DFP), $Fe(DFP)_2$ and $Fe(DFP)_3$

Table S1. The sequences of model Mim-containing peptides and the results of HPLC and ESI-MS analysis.

Peptide number	Peptide sequence	Retention time [min]	$[M+H]^+$ found *m/z*[a]	$[M+H]^+$ calculated for formula (monoisotopic) *m/z*[a]
1	H-Mim-Val-Tyr-Thr-NH_2	6.5	561.264	561.267
2	H-Asp-Mim-Tyr-Thr-NH_2	5.6	577.227	577.225
3	H-Asp-Val-Mim-Thr-NH_2	5.2	513.231	513.230
4	H-Mim-Gly-Mim-Gly-OH	4.9	492.189	492.184
5	H-Mim-Gly-Pro-Gly-Mim-Gly-OH	6.5	647.246	647.242
6	H-Mim-Gly-Pro-Gly-Mim-Gly-Gly-Mim-OH	6.2	884.319	884.317

[a] *m/z* values are presented for the monoisotopic ions

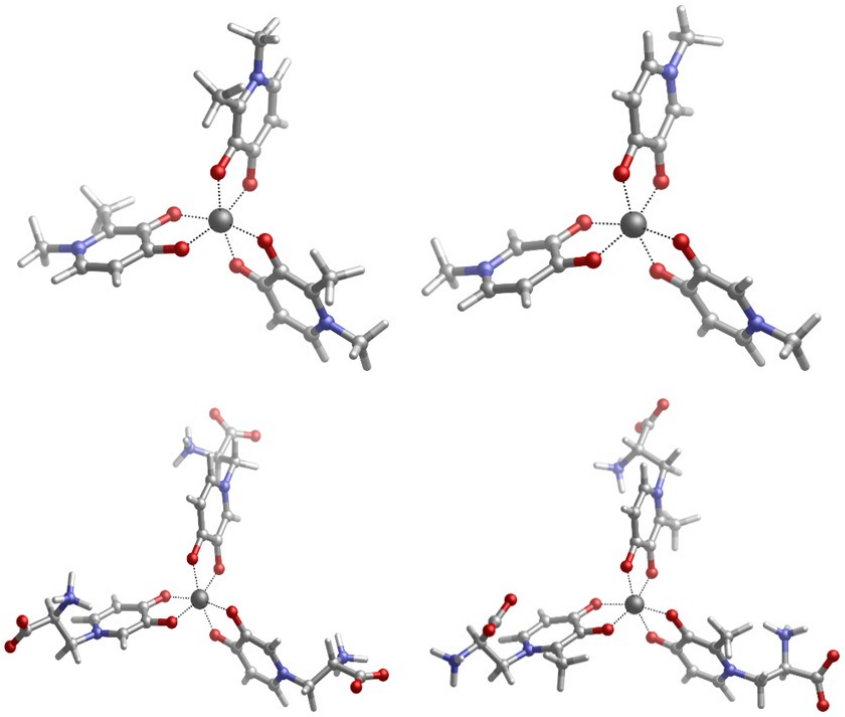

Figure S1. DFT 1:3 complexes characterized with Fe(III): Fe.$(DFP)_3$ and Fe.$(DFPunmet)_3$ (above), Fe.$(MIM)_3$ and Fe.$(MIMmet)_3$ (below).

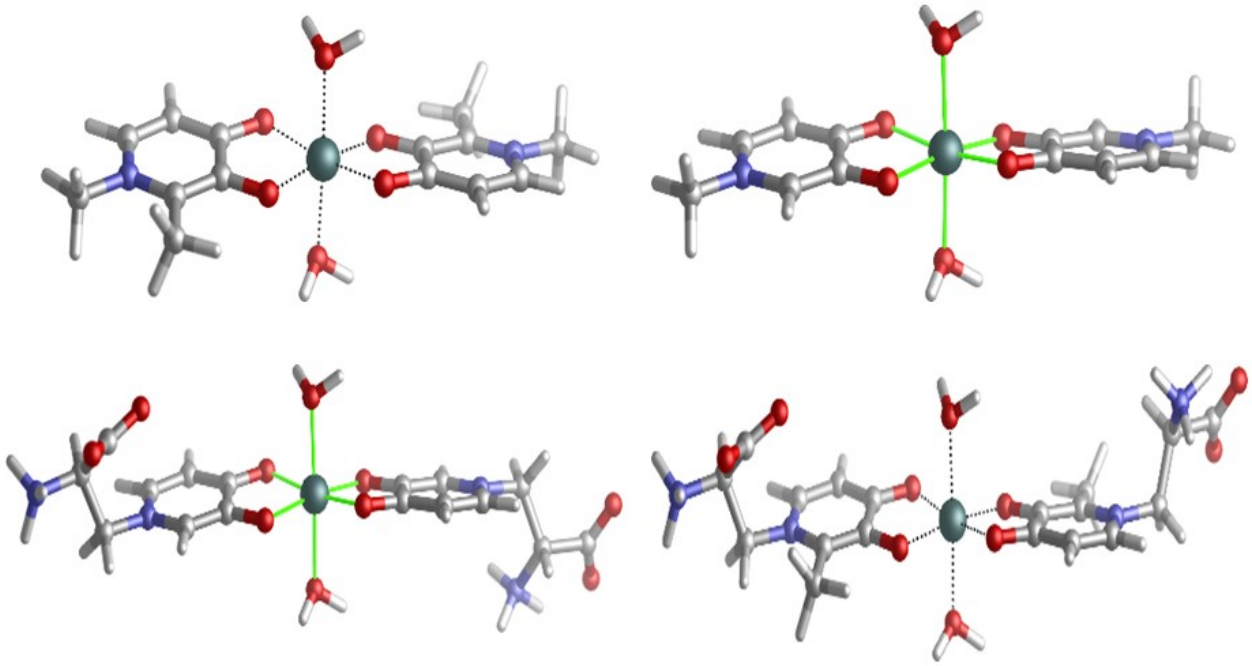

Figure S2. DFT 1:2 complexes characterized with Fe(III): Fe.$(DFP)_2$ and Fe.$(DFPunmet)_2$ (above), Fe.(MIM)3 and Fe.(MIMmet)3 (below).

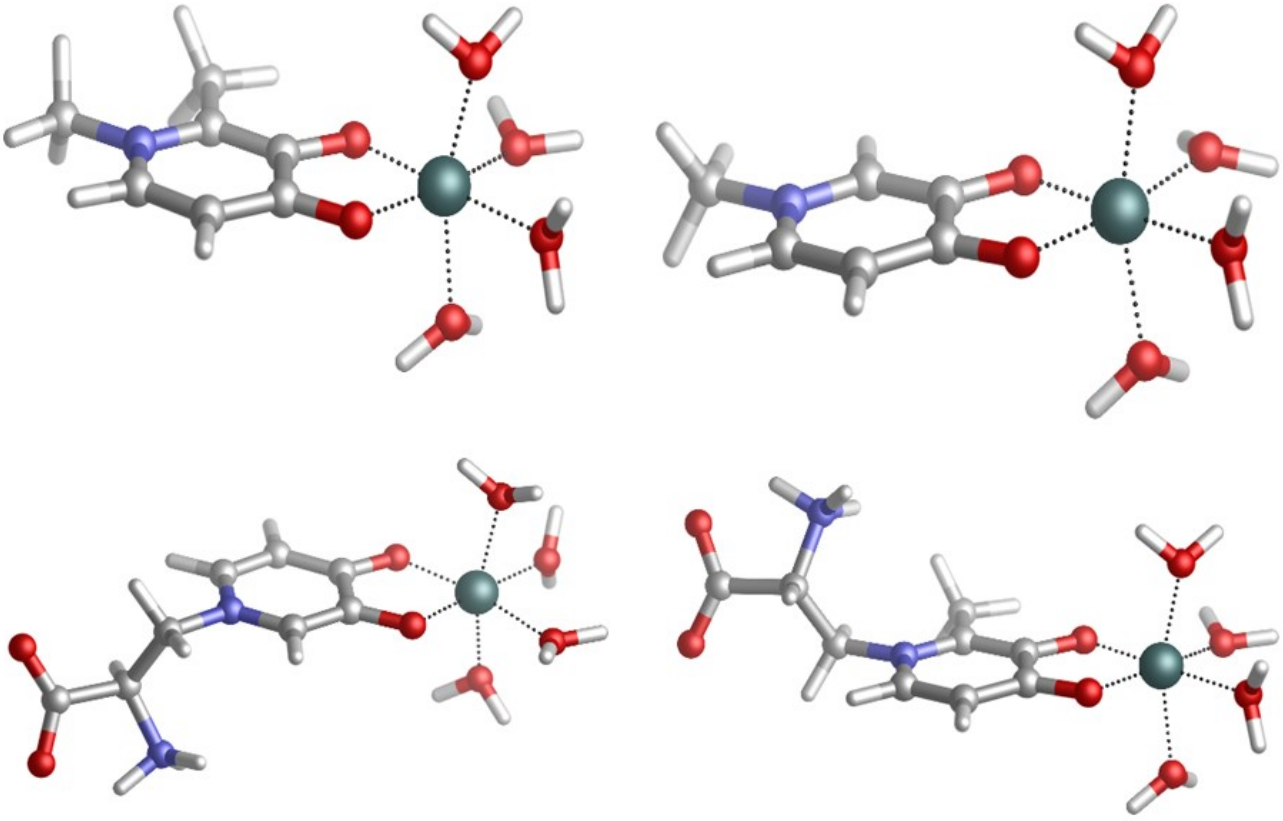

Figure S3. DFT 1:1 complexes characterized with Fe(III): Fe.(DFP) and Fe.(DFPunmet) (above), Fe.(MIM) and Fe.(MIMmet) (below).

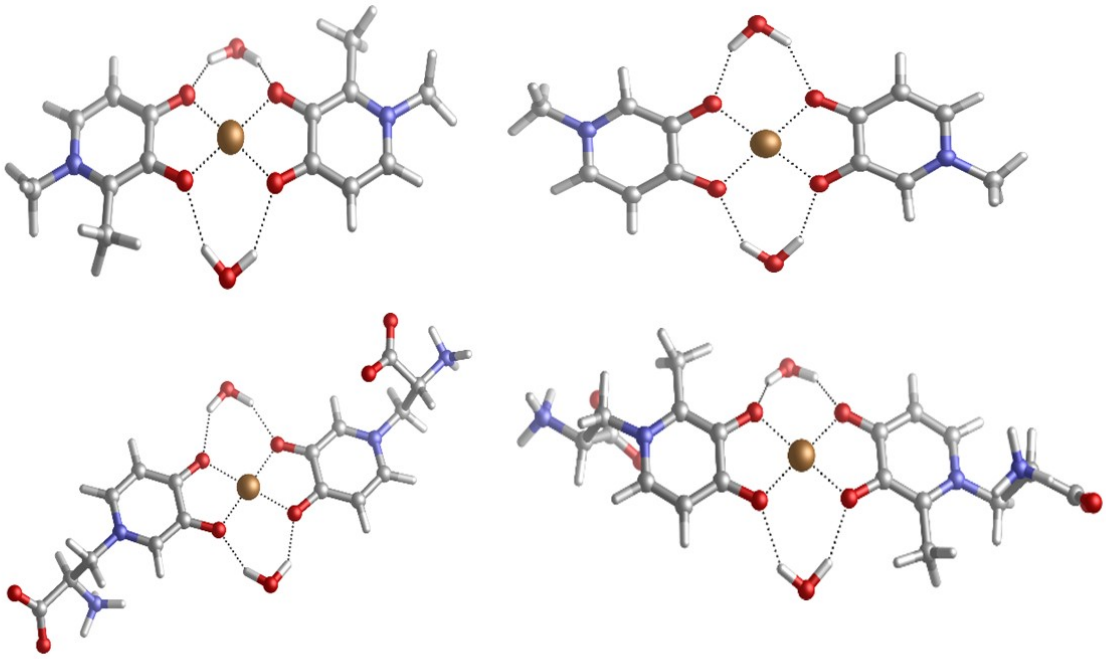

Figure S4. DFT 1:2 complexes characterized with Cu(II): Cu.$(DFP)_2$ and Cu.$(DFPunmet)_2$ (above), Cu.$(MIM)_2$ and Cu.$(MIMmet)_2$ (below).

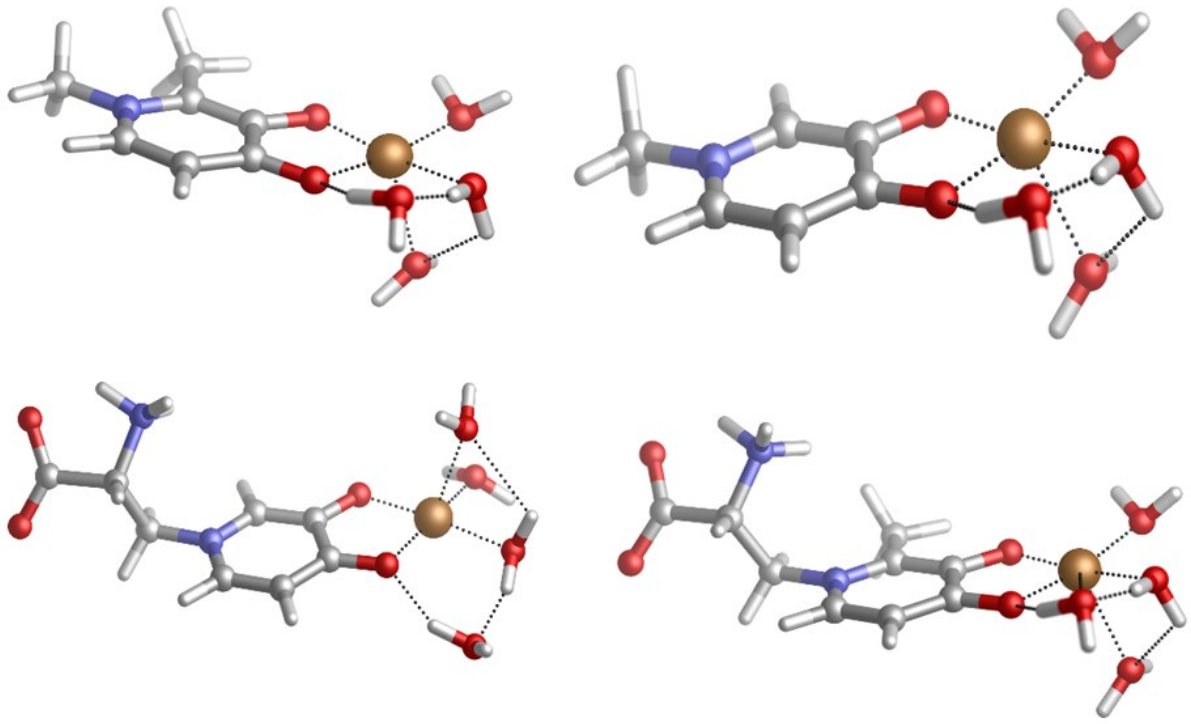

Figure S5. DFT 1:1 complexes characterized with Cu(II): Cu.(DFP) and Cu.(DFPunmet) (above), Cu.(MIM) and Cu.(MIMmet) (below).

Table S2. Computed binding enthalpies (ΔHcomp) and free energies (ΔGcomp) in solution of 1:1, 1:2 and 1:3 Fe(III):Ligand complexes and 1:1, 1:2 Cu(II):Ligand complexes, where Ligand can be: DFP, DFPunmet, MIM, MIMmet (see Scheme 2). Geometries are shown in Fig. S1 and S2. All energies are in kcal/mol and for each stoichiometry the relative free energy values were also calculated (ΔΔGcomp) taking M.(DFP)n as reference. Available experimental logβ values are also included. [a]Data taken from ref.25. [b]Data taken from ref.32. [c]Data taken from ref.31.

		ΔH_{comp}	ΔG_{comp}	$\Delta\Delta G_{comp}$	logβ
1:1 Complexes	Fe.DFP	-78.3	-81.5	**0**	**15.01[a]**
	$Fe.DFP^{unmet}$	-73.3	-77.2	**4.3**	
	Fe.MIM	-68.7	-72.3	**9.2**	**12[b]**
	$Fe.MIM^{met}$	-73.1	-76.8	**4.7**	
	Cu.DFP	-53.5	-56.1	**0**	**10.42[a]**
	$Cu.DFP^{unmet}$	-50.3	-53.4	**2.7**	
	Cu.MIM	-46.9	-50.0	**6.1**	**9.45[c]**
	$Cu.MIM^{met}$	-49.4	-52.5	**3.6**	
1:2 Complexes	$Fe(DFP)_2$	-124.6	-131.2	**0**	**27.3[a]**
	$Fe.(DFP^{unmet})_2$	-117.4	-123.2	**8.0**	
	$Fe.(MIM)_2$	-109.0	-115.8	**15.4**	**21.5[b]**
	$Fe.(MIM^{met})_2$	-117.5	-123.3	**7.9**	
	$Cu.(DFP)_2$	-88.0	-95.2	**0**	**19.09[a]**
	$Cu.(DFP^{unmet})_2$	-82.4	-91.7	**3.5**	
	$Cu.(MIM)_2$	-74.4	-82.0	**13.2**	**17.68[c]**
	$Cu.(MIM^{met})_2$	-80.5	-88.5	**6.7**	
1:3 Complexes	$Fe(DFP)_3$	-159.5	-167.4	**0**	**37.43[a]**
	$Fe.(DFP^{unmet})_3$	-151.3	-160.4	**7.0**	
	$Fe.(MIM)_3$	-143.6	-151.8	**15.6**	**29.5[b]**
	$Fe.(MIM^{met})_3$	-149.2	-156.7	**10.7**	

Table S3. ^{1}H and ^{13}C chemical shifts assigned for the Peptide1 H-Mim-Val-Tyr-Thr-NH_2 [ppm].

Res.	C^{α}	C^{β}	C^{γ}	C^{δ}	C^{ε}	$C^{ring\$}$	H^{α}	H^{β}*	H^{γ}	H^{δ}	H^{ε}	HN	H^{f}
Mim	59.41	63.82	-	-	-	114.93 128.56 136.0	3.61	3.98	-	6.39	7.11	-	7.26
Val	61.8	31.97	21.89 22.76	-	-	-	4.198	1.888	0.820 0.805	-	-	-	-
Thr	62.03	69.27	21.52	-	-	-	4.423	4.154 4.177	1.137	-	-	-	-
Thr	62.49	69.44	21.60	-	-	-	4.454	4.159	1.142	-	-	-	-

The accuracy of chemical shift determination is 0.01 ppm for ^{1}H and 0.1 ppm for ^{13}C resonances.

* Stereospecifically assigned H^{β} protons first and second values correspond to $H^{\beta 1}$ and $H^{\beta 2}$, respectively.

$ ring carbons of Mim C^{3}, C^{4} and C^{5} (up to down) are connected to the H^{δ}, H^{f} and H^{ε} protons, respectively.

^For Val C^{γ} carbons first and second values correspond to $C^{\gamma 1}$ and $C^{\gamma 2}$, respectively, analogically with the H^{γ} protons.

Table S4. ^{1}H and ^{13}C chemica shifts assigned for the Peptide2 H-Asp-Mim-Tyr-Thr-NH_2 [ppm].

Res.	C^{α}	C^{β}	C^{γ}	C^{δ}	C^{ε}	$C^{ring\$}$	H^{α}	H^{β}*	H^{γ}	H^{δ}	H^{ε}	HN	$H^{f\wedge}$
Asp	54.66	40.82	-	-	-	-	4.580	2.688	-	-	-	-	-
						114.84							
Mim	59.24	63.78	-	-	-	128.40	3.56	3.83	-	6.31	7.06	-	7.22
						136.0							
									1.970				
Tyr	58.14	39.22	-	-	-	132.55	4.512	2.846	-	-	-	-	6.931
						117.77							6.69
Thr	62.77	69.54	21.61	-	-	-	4.601	2.171	1.142	-	-	-	-

The accuracy of chemical shift determination is 0.01 ppm for ^{1}H and 0.1 ppm for ^{13}C resonances.

* Stereospecifically assigned H^{β} protons first and second values correspond to $H^{\beta 1}$ and $H^{\beta 2}$, respectively.

$ ring carbons of Mim C^{3}, C^{4} and C^{5} (up to down) are connected to the H^{δ}, H^{f} and H^{ε} protons, respectively. For Tyr they correspond to C^{δ} and C^{ε}, respectively.

^ aromatic protons in case of Tyr are shown as H^{δ} and H^{ε}, respectively, analogically the aromatic carbons C^{δ} and C^{ε}, respectively in the C^{ring} column.

Table S5. ^{1}H and ^{13}C chemical shifts assigned for the Peptide3 H-Asp-Val-Mim-Thr-NH_2 [ppm].

Res.	C^{α}	C^{β}	$C^{\gamma\wedge}$	$C^{\delta\ddot{}}$	C^{ε}	$C^{ring\$}$	H^{α}	$H^{\beta*}$	$H^{\gamma\wedge}$	H^{δ}	H^{ε}	HN	H^{f}
Asp	54.59	40.79	-	-	-	-	4.571	2.677	-	-	-	-	-
Val	61.7	32.00	21.84 22.72	-	-	-	4.186	1.901	0.819 0.808 1.970	-	-	-	-
Mim	59.20	63.75	-	-	-	114.88 128.44 136.1	3.53	3.82	-	6.34	7.08	-	7.19
Thr	62.71	69.58	21.58	-	-	-	4.593	2.168	1.140	-	-	-	-

The accuracy of chemical shift determination is 0.01 ppm for ^{1}H and 0.1 ppm for ^{13}C resonances.

* Stereospecifically assigned H^{β} protons first and second values correspond to $H^{\beta1}$ and $H^{\beta2}$, respectively.

$ ring carbons of Mim C^{3}, C^{4} and C^{5} (up to down) are connected to the H^{δ}, H^{f} and H^{ε} protons, respectively.

^For Val C^{γ} carbons first and second values correspond to $C^{\gamma1}$ and $C^{\gamma2}$, respectively, analogically with the H^{γ} protons.

Table S6. ^{1}H and ^{13}C chemical shifts assigned for the Peptide4 H-Mim-Gly-Mim-Gly-OH [ppm].

Res.	C^{α}	C^{β}	C^{γ}	C^{δ}	C^{ε}	$C^{ring\$}$	$H^{\alpha*}$	$H^{\beta*}$	H^{γ}	H^{δ}	H^{ε}	HN	$H^{f\wedge}$
Mim1	59.43	63.80	-	-	-	115.01 128.61 136.12	3.66	4.01	-	6.41	7.13	-	7.30
Gly1	45.11	-	-	-	-	-	3.92 3.90	-	-	-	-	8.22	-
Mim2	59.31	63.69	-	-	-	114.95 128.55 136.04	3.61	3.97	-	6.33	7.05	-	7.24
Gly2	45.31	-	-	-	-	-	3.96	-	-	-	-	-	-

The accuracy of chemical shift determination is 0.01 ppm for ^{1}H and 0.1 ppm for ^{13}C resonances.

* Stereospecifically assigned H^{β} protons first and second values correspond to $H^{\beta1}$ and $H^{\beta2}$, respectively. For glycines they correspond to $H^{\alpha2}$ and $H^{\alpha3}$, respectively.

$ ring carbons of Mim C^{3}, C^{4} and C^{5} (up to down) are connected to the H^{δ}, H^{f} and H^{ε} protons, respectively.

Table S7. ^{1}H and ^{13}C chemical shifts assigned for the Peptide5 H-Mim-Gly-Pro-Gly-Mim-Gly-OH [ppm].

Res.	C^{α}	C^{β}	C^{γ}	C^{δ}	C^{ε}	$C^{ring\$}$	H^{α}	H^{β}*	H^{γ}	H^{δ}	H^{ε}	HN	$H^{f\wedge}$
Mim1	59.43	63.80	-	-	-	115.01 128.61 136.12	3.69	4.08	-	6.40	7.13	-	7.32
Gly1	45.09	-	-	-	-	-	3.91 3.93	-	-	-	-	8.19	-
Pro	62.93	31.19	26.98	49.62	-	-	4.353	2.101 2.133	-	3.690	-	-	-
Gly2	45.11	-	- 15.59	-	-	-	3.90	-	- 1.279 0.851	-	-	8.159	-
Mim2	59.54	63.85	-	-	-	115.11 128.44 135.98	3.64	4.05	-	6.37	7.08	-	7.27
Gly3	45.35	-	-	-	-	-	-	-	-	-	-	-	-

The accuracy of chemical shift determination is 0.01 ppm for ^{1}H and 0.1 ppm for ^{13}C resonances.

* Stereospecifically assigned H^{β} protons first and second values correspond to $H^{\beta 1}$ and $H^{\beta 2}$, respectively. For glycines they correspond to $H^{\alpha 2}$ and $H^{\alpha 3}$, respectively.

$ ring carbons of Mim C^{3}, C^{4} and C^{5} (up to down) are connected to the H^{δ}, H^{f} and H^{ε} protons, respectively.

Table S8. 1:3 Fe(III)-DFP crystallographic data compared with DFT optimized geometries of metal coordination core. Optimizations carried out at the B3LYP-D3(BJ)/6-31++(g,d) IEFPCM level of theory. A, B and C distinguish different MIM amino acids, while p (para) and m (meta) is the oxygen (carbonyl and hydroxyl) position respect to the nitrogen in the pyridinone ring.

			Fe-DFP$_3$ (exp)[1]	**Fe-DFP$_3$ (comp)**
atom1	**atom2**		**Distances**	
Fe	O^A_p		2.046	2.083
Fe	O^A_m		1.999	2.004
Fe	O^B_p		2.045	2.083
Fe	O^B_m		1.997	2.003
Fe	O^C_p		2.046	2.084
Fe	O^C_m		1.997	2.003
atom1	**atom2**	**atom3**	**Angles**	
Fe	O^A_p	C^A_p	112.1	112.2
Fe	O^A_m	C^A_m	111.9	114.3
Fe	O^B_p	C^B_p	112.1	112.2
Fe	O^B_m	C^B_m	111.9	114.3
Fe	O^C_p	C^C_p	112.1	112.1
Fe	O^C_m	C^C_m	111.9	114.4
O^A_p	Fe	O^A_m	80.7	79.8
O^A_p	Fe	O^B_p	90.2	89.0
O^A_p	Fe	O^B_m	98.4	98.9
O^A_p	Fe	O^C_p	90.2	88.8
O^A_p	Fe	O^C_m	167.4	165.9
O^A_m	Fe	O^B_p	167.5	166.3
O^A_m	Fe	O^B_m	91.9	93.9
O^A_m	Fe	O^C_p	98.4	98.8
O^A_m	Fe	O^C_m	91.9	93.7
O^B_p	Fe	O^B_m	80.8	79.8
O^B_p	Fe	O^C_p	90.2	88.9
O^B_p	Fe	O^C_m	98.5	98.9
O^B_m	Fe	O^C_p	167.5	166.2
O^B_m	Fe	O^C_m	92.0	93.9
O^C_p	Fe	O^C_m	80.8	79.8

(1) Crystal structure CCDC (JAWSEF01, additional database identifier JUHXEP, 1183333) of Fe(DFO)$_3$ complexes by E.T.Clarke et al. (E.T.Clarke, A.E.Martell, J.Reibenspies, Inorganica Chimica Acta, 1992, 196, 177, DOI: 10.1016/S0020-1693(00)86121-6)

Table S9. 1:2 Cu(II)-DFP crystallographic data compared with DFT optimized geometries of metal coordination core. Optimizations carried out at the B3LYP-D3(BJ)/6-31++(g,d) IEFPCM level of theory. A, B and C distinguish different MIM amino acids, while p (para) and m (meta) is the oxygen (carbonyl and hydroxyl) position respect to the nitrogen in the pyridinone ring.

			Cu-DFP$_2$ (exp)[1]	**Cu-DFP$_2$ (comp)**
atom1	**atom2**		**Distances**	
Cu	O^A_p		1.913	1.940
Cu	O^A_m		1.928	1.959
Cu	O^B_p		1.913	1.940
Cu	O^A_m		1.928	1.959
atom1	**atom2**	**atom3**	**Angles**	
Cu	O^A_p	C^A_p	108.5	110.5
Cu	O^A_m	C^A_m	110.3	110.5
Cu	O^B_p	C^B_p	108.5	110.5
Cu	O^B_m	C^B_m	110.3	110.5
O^A_p	Cu	O^A_m	86.1	84.9
O^A_p	Cu	O^B_p	180.0	178.0
O^A_p	Cu	O^B_m	93.9	95.1
O^A_m	Cu	O^B_p	93.9	95.1
O^A_m	Cu	O^B_m	180.0	175.9
O^B_p	Cu	O^B_m	86.1	84.9

(1) The crystal structure (CCDC: 1291877, WELTEM) of $Cu(DFO)_2$ complex by A.El-Jammal et al. (A.El-Jammal, P.L.Howell, M.A.Turner, Naiyin Li, D.M.Templeton J.Med.Chem., 37, 1994, 461; DOI: 10.1021/jm00030a005).

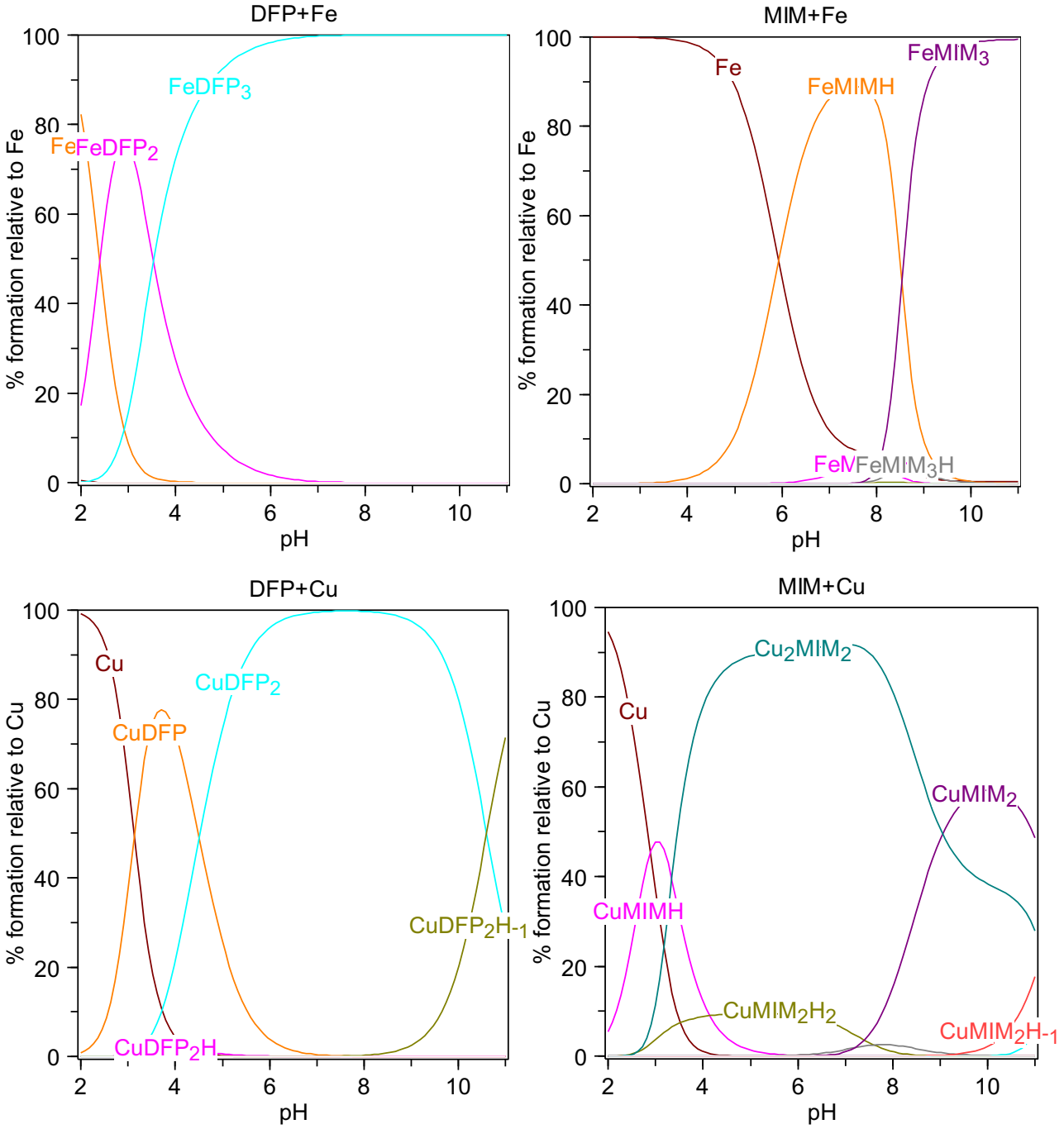

Figure S6. Speciation plots of DFP and MIM with iron ions (up; [DFP]=1.0×10^{-3} [M]; [Fe^{3+}]=3.3×10^{-4} [M] and [MIM]=1.0×10^{-3} [M]) and with copper ions (down; [DFP]=1.00×10^{-3} [M]; [Cu^{2+}]=5×10^{-4} [M] and [MIM]=1×10^{-3} [M]). Metal complexes calculated on the basis of stability constants reported in Ref. 32 (DFP with Fe^{3+} and Cu^{2+}), 58 (MIM with Fe^{3+}) and 38 (MIM complexes with Cu^{2+}). Charges are omitted for simplicity.

Table S10. 1:2 Cu(II)-DFP crystallographic data compared with 2:2 Cu(II)-MIM and 2:2 Cu(II)-P2 DFT optimized geometries of metal coordination core. Optimizations carried out at the B3LYP-D3(BJ)/6-31++(g,d) IEFPCM level of theory. A and B distinguish ligand binding sites in different ligands, while p (para) and m (meta) is the oxygen (carbonyl and hydroxyl) position respect to the nitrogen in the pyridinone ring.

			Cu-DFP$_2$ (exp)[1]				**Cu$_2$Mim$_2$**				**Cu$_2$(P2)$_2$**
atom1	**atom2**		**Distances**	**atom1**	**atom2**		**Distances**	**atom1**	**atom2**		**Distances**
Cu	O^A_p		1.913	Cu1	N^B		2.025	Cu1	N^B		1.995
Cu	O^A_m		1.928	Cu1	O^B		1.970	Cu1	O^B		1.929
Cu	O^B_p		1.913	Cu1	O^A_p		1.963	Cu1	O^A_p		1.979
Cu	O^B_m		1.928	Cu1	O^A_m		1.942	Cu1	O^A_m		1.932
				Cu1	O_{W1}		2.465				
				Cu2	O^B_p		1.963	Cu2	O^B_p		1.97
				Cu2	O^B_m		1.942	Cu2	O^B_m		1.968
				Cu2	N^A		2.025	Cu2	N^A		2.007
				Cu2	O^A		1.970	Cu2	O^A		1.959
				Cu1	O_{W2}		2.465	Cu1	O^{asp}		2.558
atom1	**atom2**	**atom3**	**Angles**	**atom1**	**atom2**	**atom3**	**Angles**	**atom1**	**atom2**	**atom3**	**Angles**
O^A_p	Cu	O^A_m	86.1	N^B	Cu1	O^B	82.1	N^B	Cu1	O^B	95.7
O^A_p	Cu	O^B_m	93.9	N^B	Cu1	O^A_p	95.9	N^B	Cu1	O^A_p	156.6
O^A_p	Cu	O^B_p	180.0	N^B	Cu1	O^A_m	173.2	N^B	Cu1	O^A_m	90.5
O^A_m	Cu	O^B_m	180.0	O^B	Cu1	O^A_p	171.7	O^B	Cu1	O^A_p	95.0
O^A_m	Cu	O^B_p	93.9	O^B	Cu1	O^A_m	95.4	O^B	Cu1	O^A_m	162.2
O^B_p	Cu	O^B_m	86.1	O^A_p	Cu1	O^A_m	85.6	O^A_p	Cu1	O^A_m	85.5
				OW1	Cu1	O^A_m	102.5				
				OW2	Cu1	O^A_p	93.68				
				OW3	Cu1	N^B	84.42				
				OW4	Cu1	O^B	94.19				
				O^B_p	Cu2	O^B_m	85.6	O^B_p	Cu2	O^B_m	84.9
				O^B_p	Cu2	N^A	95.9	O^B_p	Cu2	N^A	170.4
				O^B_p	Cu2	O^A	171.7	O^B_p	Cu2	O^A	92.1
				O^B_m	Cu2	N^A	173.2	O^B_m	Cu2	N^A	92.2
				O^B_m	Cu2	O^A	95.4	O^B_m	Cu2	O^A	155.8
				N^A	Cu2	O^A	82.1	N^A	Cu2	O^A	94.2
				O_{W2}	Cu2	O^B_m	102.15	O^{asp}	Cu2	NA	70.79
				O_{W2}	Cu2	O^B_p	93.68	O^{asp}	Cu2	OA	82.58
				O_{W2}	Cu2	N^A	91.42	O^{asp}	Cu2	O^B_p	102.96
				O_{W2}	Cu2	O^A	94.19	O^{asp}	Cu2	O^B_m	121.5

(1) The crystal structure (CCDC: 1291877, WELTEM) of Cu(DFO)$_2$ complex by A.El-Jammal et al. (A.El-Jammal, P.L.Howell, M.A.Turner, Naiyin Li, D.M.Templeton J.Med.Chem., 37, 1994, 461; DOI: 10.1021/jm00030a005).

Table S11. 1:1 Fe(III)-peptide DFT optimized geometries data of metal coordination core. Optimizations carried out at the B3LYP-D3(BJ)/6-31++(g,d) IEFPCM level of theory. A, B and C distinguish different MIM amino acids in the peptide, while p (para) and m (meta) is the oxygen (carbonyl or hydroxyl) position respect to the nitrogen in the pyridinone ring. W refers to water molecule.

			Fe-Pep[4]	**Fe-Pep[5]**	**Fe-Pep[6]**
atom1	**atom2**		**Distances**		
Fe	O^{A}_{p}		2.055	2.019	2.107
Fe	O^{A}_{m}		1.955	1.984	2.014
Fe	O^{B}_{p}		2.034	2.044	2.102
Fe	O^{B}_{m}		1.957	1.963	2.012
Fe	O^{C}_{p}/W_1		2.140	2.181	2.069
Fe	O^{C}_{m}/W_2		2.167	2.125	1.993
atom1	**atom2**	**atom3**	**Angles**		
Fe	O^{A}_{p}	C	110.5	109.5	108.7
Fe	O^{A}_{m}	C	112.6	103.17	110.5
Fe	O^{B}_{p}	C	107.8	108.0	110.0
Fe	O^{B}_{m}	C	108.6	108.9	112.2
Fe	O^{C}_{p}/W_1	C	-	-	111.4
Fe	O^{C}_{m}/W_2	C	-	-	80.0
O^{A}_{p}	Fe	O^{A}_{m}	81.1	81.1	79.3
O^{A}_{p}	Fe	O^{B}_{p}	90.9	87.5	87.9
O^{A}_{p}	Fe	O^{B}_{m}	166.8	110.1	89.2
O^{A}_{p}	Fe	O^{C}_{p}/W_1	98.2	155.9	170.3
O^{A}_{p}	Fe	O^{C}_{m}/W_2	79.3	104.7	97.3
O^{A}_{m}	Fe	O^{B}_{p}	95.3	103.9	85.2
O^{A}_{m}	Fe	O^{B}_{m}	88.6	168.1	161.0
O^{A}_{m}	Fe	O^{C}_{p}/W_1	97.2	78.7	92.1
O^{A}_{m}	Fe	O^{C}_{m}/W_2	159.5	90.9	105.9
O^{B}_{p}	Fe	O^{B}_{m}	81.8	81.2	79.4
O^{B}_{p}	Fe	O^{C}_{p}/W_1	165.5	84.7	95.9
O^{B}_{p}	Fe	O^{C}_{m}/W_2	90.9	162.3	168.5
O^{B}_{m}	Fe	O^{C}_{p}/W_1	91.2	91.1	100.3
O^{B}_{m}	Fe	O^{C}_{m}/W_2	111.7	82.5	90.4
O^{C}_{p}/W_1	Fe	O^{C}_{m}/W_2	79.9	88.7	80.7

Table S12. 1:1 Cu(II)-peptide DFT optimized geometries data of metal coordination core. Optimizations carried out at the B3LYP-D3(BJ)/6-31++(g,d) IEFPCM level of theory. A and B distinguish different MIM amino acids in the peptide, while p (para) and m (meta) is the oxygen (carbonyl or hydroxyl) position respect to the nitrogen in the pyridinone ring. W refers to water molecule.

			Cu-Pep[4]	**Cu-Pep[5]**	**Cu-Pep[6]**
atom1	**atom2**		**Distances**		
Cu	O^A_p		1.993	2.507	2.804
Cu	O^A_m		1.946	1.920	1.976
Cu	O^B_p		3.286	2.027	2.006
Cu	O^B_m		1.928	1.921	2.003
Cu	O^C_p/W_1		2.460	2.082	2.413
Cu	O^C_m/W_2		2.044	2.987	1.972
atom1	**atom2**	**atom3**	**Angles**		
Cu	O^A_p	C	108.7	97.2	92.8
Cu	O^A_m	C	109.2	113.3	114.1
Cu	O^B_p	C	81.8	107.0	109.9
Cu	O^B_m	C	114.3	108.6	109.4
Cu	O^C_p/W_1	C	-	-	103.9
Cu	O^C_m/W_2	C	-	-	116.0
O^A_p	Cu	O^A_m	85.2	74.8	68.9
O^A_p	Cu	O^B_p	117.4	81.2	79.8
O^A_p	Cu	O^B_m	175.6	112.6	95.1
O^A_p	Cu	O^C_p/W_1	79.3	116.4	164.3
O^A_p	Cu	O^C_m/W_2	91.1	144.2	103.1
O^A_m	Cu	O^B_p	115.1	103.0	91.2
O^A_m	Cu	O^B_m	95.1	170.4	163.8
O^A_m	Cu	O^C_p/W_1	103.3	87.1	95.4
O^A_m	Cu	O^C_m/W_2	162.5	86.0	94.7
O^B_p	Cu	O^B_m	58.5	84.6	93.3
O^B_p	Cu	O^C_p/W_1	138.6	161.7	101.1
O^B_p	Cu	O^C_m/W_2	52.2	73.9	174.0
O^B_m	Cu	O^C_p/W_1	104.9	84.1	100.6
O^B_m	Cu	O^C_m/W_2	87.4	90.6	91.1
O^C_p/W_1	Cu	O^C_m/W_2	92.7	91.9	77.6

Table S13. 2:2 Cu(II)-peptide DFT optimized geometries data of metal coordination core. Optimizations carried out at the B3LYP-D3(BJ)/6-31++(g,d) IEFPCM level of theory. A1 and B1 distinguish different MIM amino acids in the first peptide in the dimer complex and A2 and B2 distinguish MIM amino acids in the second peptide in the dimer complex, while p (para) and m (meta) is the oxygen (carbonyl or hydroxyl) position respect to the nitrogen in the pyridinone ring.

			Cu-P4				**Cu-P5**
atom1	**atom2**		**Distances**	**atom1**	**atom2**		**Distances**
Cu1	$O^{B2}{}_{p}$		1.955	Cu1	$O^{B2}{}_{p}$		1.963
Cu1	$O^{B2}{}_{m}$		1.942	Cu1	$O^{B2}{}_{m}$		1.947
Cu1	$O^{A1}{}_{p}$		1.957	Cu1	$O^{A1}{}_{p}$		1.972
Cu1	$O^{A1}{}_{m}$		1.945	Cu1	$O^{A1}{}_{m}$		1.951
Cu2	$O^{A2}{}_{p}$		1.957	Cu2	$O^{A2}{}_{p}$		1.953
Cu2	$O^{A2}{}_{m}$		1.945	Cu2	$O^{A2}{}_{m}$		1.952
Cu2	$O^{B1}{}_{p}$		1.954	Cu2	$O^{B1}{}_{p}$		1.967
Cu2	$O^{B1}{}_{m}$		1.942	Cu2	$O^{B1}{}_{m}$		1.914
atom1	**atom2**	**atom3**	**Angles**	**atom1**	**atom2**	**atom3**	**Angles**
$O^{A2}{}_{p}$	Cu1	$O^{A2}{}_{m}$	85.4	$O^{A2}{}_{p}$	Cu1	$O^{A2}{}_{m}$	85.2
$O^{A2}{}_{p}$	Cu1	$O^{B1}{}_{p}$	93.4	$O^{A2}{}_{p}$	Cu1	$O^{B1}{}_{p}$	96.0
$O^{A2}{}_{p}$	Cu1	$O^{B1}{}_{m}$	175.5	$O^{A2}{}_{p}$	Cu1	$O^{B1}{}_{m}$	172.7
$O^{A2}{}_{m}$	Cu1	$O^{B1}{}_{p}$	177.3	$O^{A2}{}_{m}$	Cu1	$O^{B1}{}_{p}$	178.3
$O^{A2}{}_{m}$	Cu1	$O^{B1}{}_{m}$	95.8	$O^{A2}{}_{m}$	Cu1	$O^{B1}{}_{m}$	93.3
$O^{B1}{}_{p}$	Cu1	$O^{B1}{}_{m}$	85.6	$O^{B1}{}_{p}$	Cu1	$O^{B1}{}_{m}$	85.6
$O^{B2}{}_{p}$	Cu2	$O^{B2}{}_{m}$	85.6	$O^{B2}{}_{p}$	Cu2	$O^{B2}{}_{m}$	85.5
$O^{B2}{}_{p}$	Cu2	$O^{A1}{}_{p}$	93.2	$O^{B2}{}_{p}$	Cu2	$O^{A1}{}_{p}$	95.6
$O^{B2}{}_{p}$	Cu2	$O^{A1}{}_{m}$	177.5	$O^{B2}{}_{p}$	Cu2	$O^{A1}{}_{m}$	172.8
$O^{B2}{}_{m}$	Cu2	$O^{A1}{}_{p}$	175.8	$O^{B2}{}_{m}$	Cu2	$O^{A1}{}_{p}$	175.8
$O^{B2}{}_{m}$	Cu2	$O^{A1}{}_{m}$	95.9	$O^{B2}{}_{m}$	Cu2	$O^{A1}{}_{m}$	94.4
$O^{A1}{}_{p}$	Cu2	$O^{A1}{}_{m}$	85.4	$O^{A1}{}_{p}$	Cu2	$O^{A1}{}_{m}$	85.0

Table S14. Antimicrobial screening of mimosine derived peptides evaluated using by the agar plate disk diffusion method.

	Microbial strains				
	Diameter of inhibition zone (mm)				
Peptides	*S. aureus* ATCC 25923	*B. cereus* ATCC 11778	*E. coli* ATCC 25922	*M. canis* 10D	*T. rubrum* 11D
P1 (50 μg/disc)	0.0±0.0	0.0±0.0	0.0±0.0	0.0±0.0	0.0±0.0
P2 (84 μg/disc)	0.0±0.0	0.0±0.0	0.0±0.0	0.0±0.0	0.0±0.0
P3 (340 μg/disc)	1.2±0.3	0.0±0.0	0.0±0.0	0.00	0.00
P4 (149 μg/disc)	0.0±0.0	0.0±0.0	0.0±0.0	0.0±0.0	0.0±0.0
P5 (810 μg/disc)	15.2±0.1	15.3±0.1	0.0±0.0	0.0±0.0	0.0±0.0
P6 (140 μg/disc)	0.0±0.0	0.0±0.0	0.0±0.0	0.0±0.0	0.0±0.0
Amoxicillin (25 μg/disc)	28.2±0.2	25.3±0.4	NT	NT	NT
Ketoconazole (15μg/disc)	NT	NT	NT	25±0.1	22±0.1

Data are means of three replicates (n = 3)± standard deviation; NT, not tested

Table S15. Minimum inhibitory concentration (MIC) and minimum bactericidal concentration (MBC) of the mimosine-peptides (μg/mL).

Peptides	***S. aureus* ATCC 25923**		***B. cereus* ATCC 11778**		***E. coli* ATCC 25922**	
	MIC	**MBC**	**MIC**	**MBC**	**MIC**	**MBC**
P3	3390	>3390	>3390	>3390	>3390	>3390
P4	> 7450	> 7450	7450	> 7450	> 7450	> 7450
P5	8100	>8100	>8100	>8100	>8100	>8100
P6	6900	>6900	>6900	>6900	>6900	>6900

Table S16. Minimum inhibitory concentration (MIC) and minimum bactericidal concentration (MBC) of the mimosine-peptides iron complexes (μg/mL).

Peptides	***S. aureus* ATCC 25923**		***B. cereus* ATCC 11778**		***E. coli* ATCC 25922**	
	MIC	**MBC**	**MIC**	**MBC**	**MIC**	**MBC**
P1-Fe	334.0	>334.0	>334.0	>334.0	>334.0	>334.0
P2-Fe	>560	>560	>560	>560	>560	>560
P4-Fe	484.0	>967.5	484.0	967.5	967.5	>967.5
P6-Fe	448.0	>896.0	448.0	448.0	896.0	>896.0

Table S17. MIC activity of Peptide 6 with and without iron.

	Peptide 6		**Ofloxacin**
Strain	**+ Fe**	**- Fe**	**- Fe**
S aureus	>1 mM	>1 mM	0,016
S. intermedius	>1 mM	>1 mM	0,031
P. aeruginosa	>1 mM	>1 mM	0,031

Table S18. Biofilm inhibition activity of Peptide 6 with and without iron.

% Biofilm inibhtion [mM]		1,000	0,500	0,250	0,125	0,063	0,031	0,016	0,008	0,004	0,002
Strain		**% Biofilm**									
S. aureus	**-Fe**	31	45	57	77	100	100	100	100	100	100
	+Fe	30	46	52	91	100	100	100	100	100	100
S. intermedius	**-Fe**	67	98	76	70	85	88	88	88	88	88
	+Fe	53	75	86	73	73	72	78	78	86	86
P. aeruginosa	**-Fe**	67	65	92	100	100	100	100	100	100	100
	+Fe	56	51	78	73	72	73	85	104	39	97

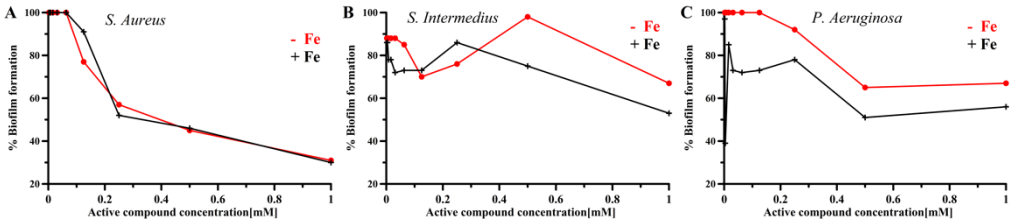

Figure S7. Graphical representation of biofilm inhibition activity of Peptide 6 with and without iron (Table S16).

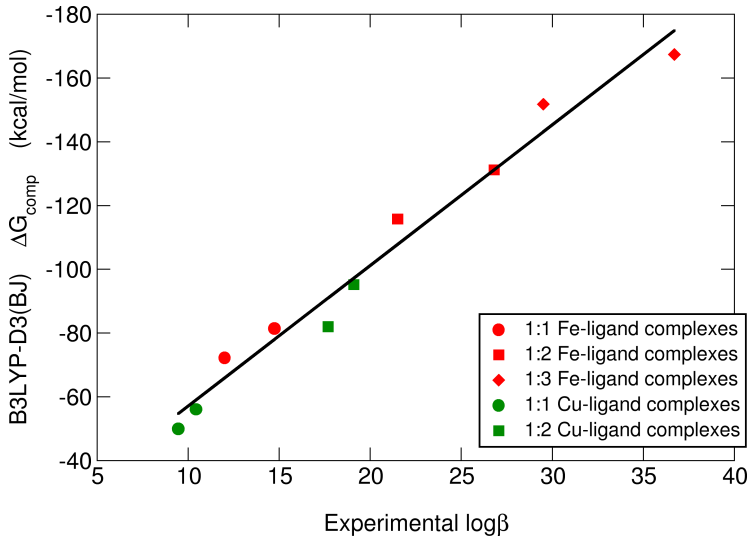

Figure S8. Computed binding energies in solution (ΔG_{comp}, in kcal/mol) versus experimental stability constants (logβ) of 1:1, 1:2 and 1:3 Fe(III):Ligand complexes and 1:1 1:2 Cu(II):Ligand complexes, where Ligand can be either DFP or MIM. The correlation coefficient (r) is 0.9873.

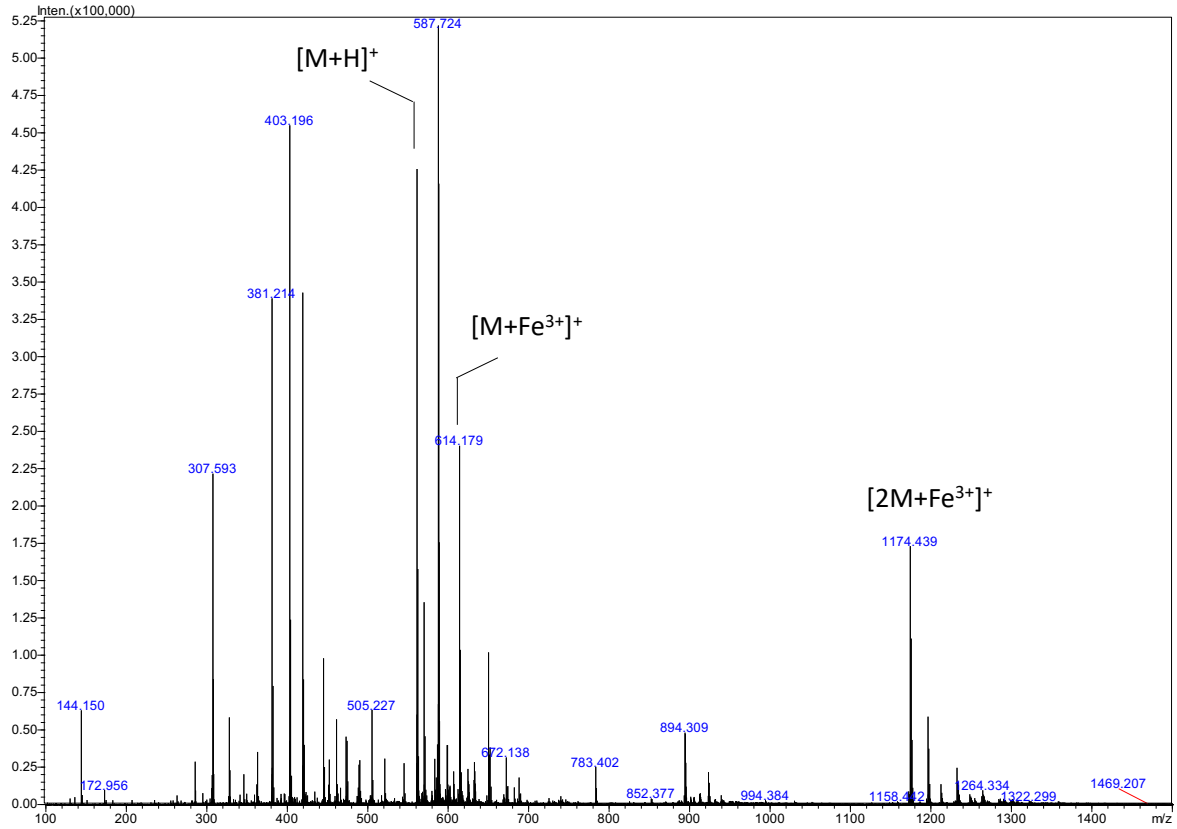

Figure S9. ESI-MS spectrum of peptide 1 complex with Fe(III) ions.

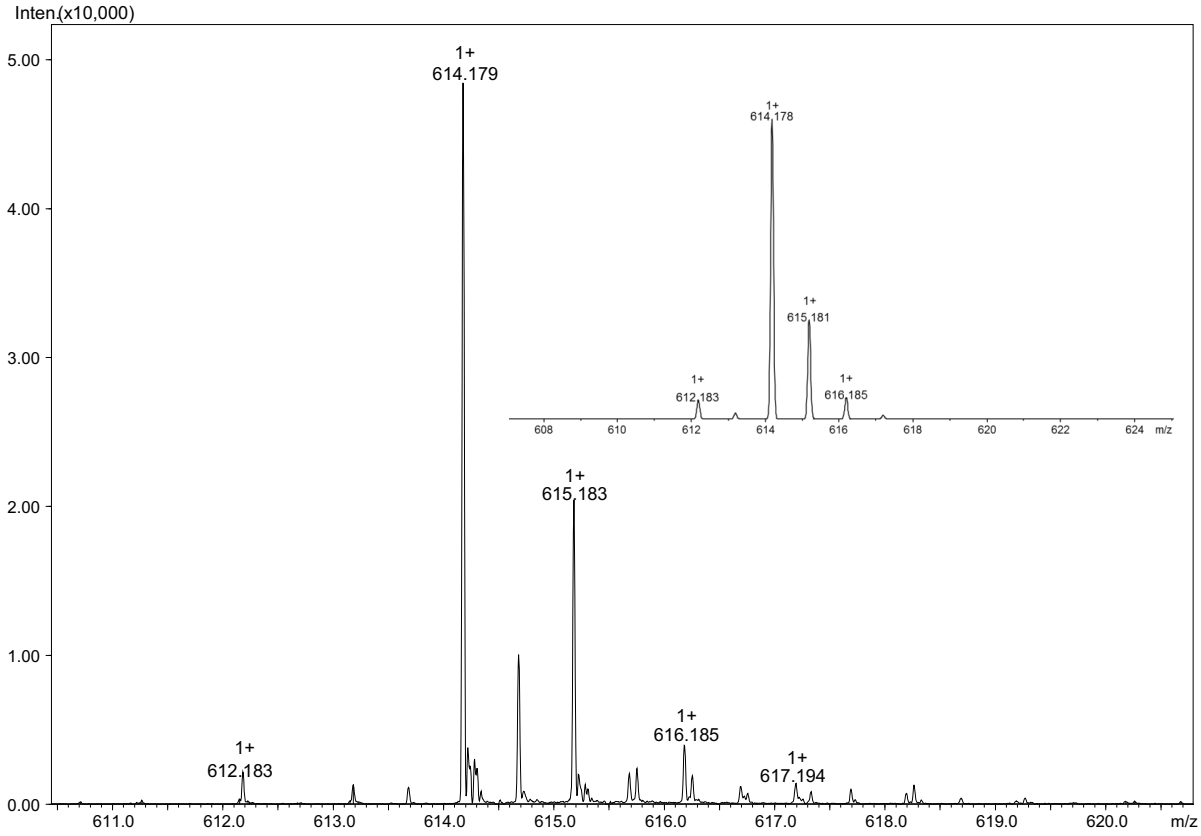

Figure S9a. Enlarged fragment of the ESI-MS spectrum of $[Fe(P1)H_{-1}]^+$ complex. Inlet presents the generated isotopic distribution for the $C_{26}H_{34}FeN_6O_8$ ion.

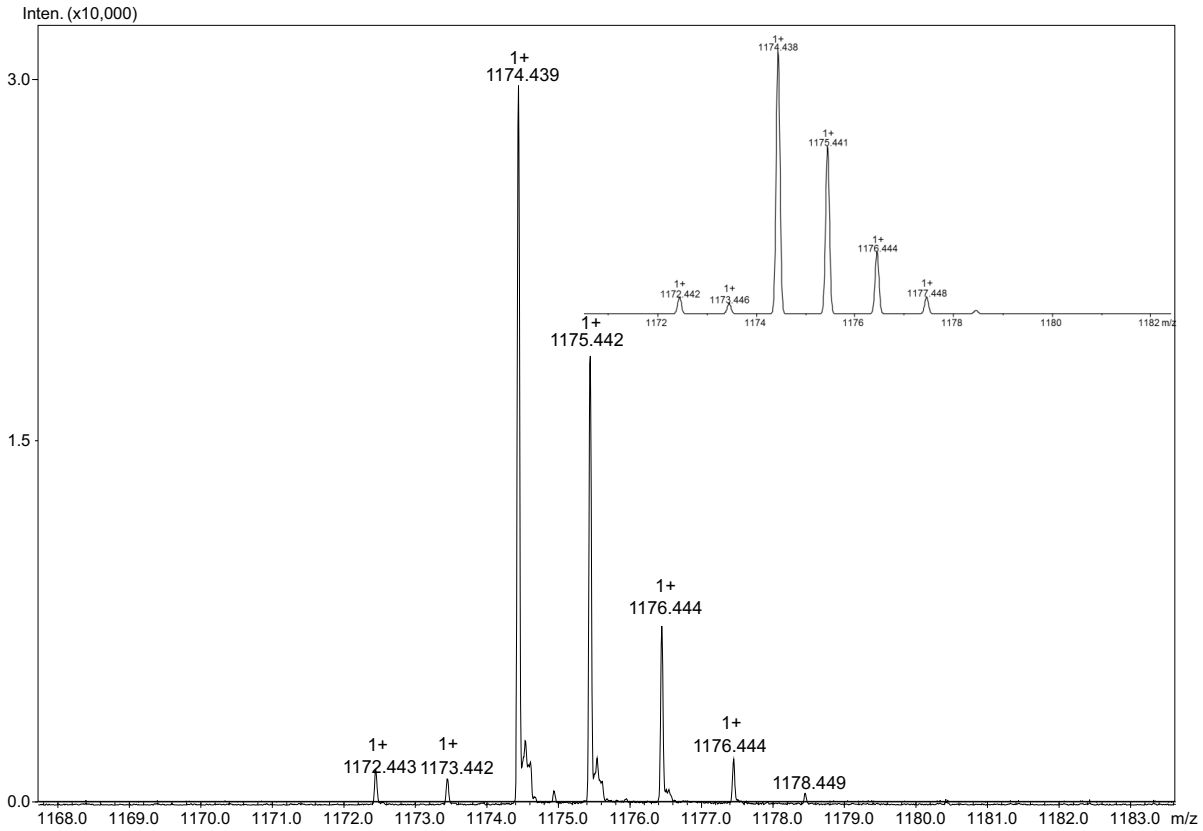

Figure S9b. Enlarged fragment of the ESI-MS spectrum of $[Fe(P1)_2]^+$ complex. Inlet presents the generated isotopic distribution for the $C_{52}H_{70}FeN_{12}O_{16}$ ion.

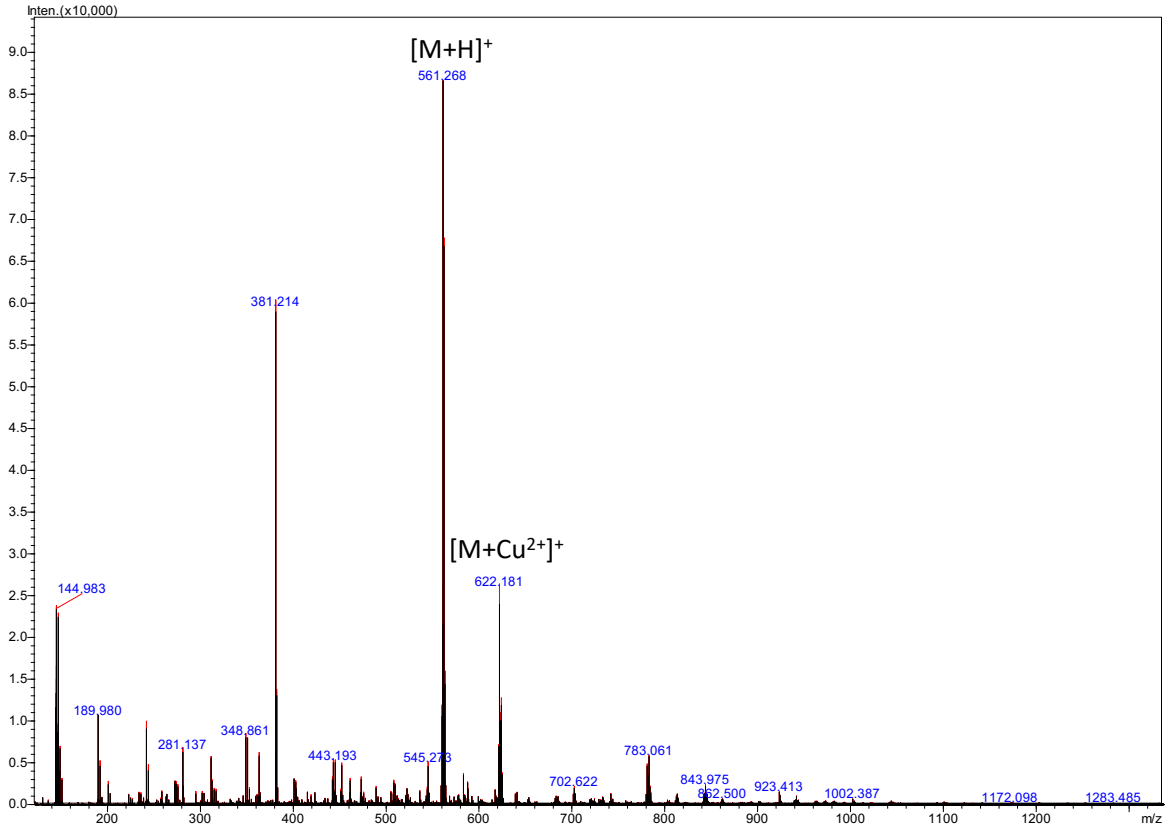

Figure S10. ESI-MS spectrum of peptide 1 complex with Cu(II) ions.

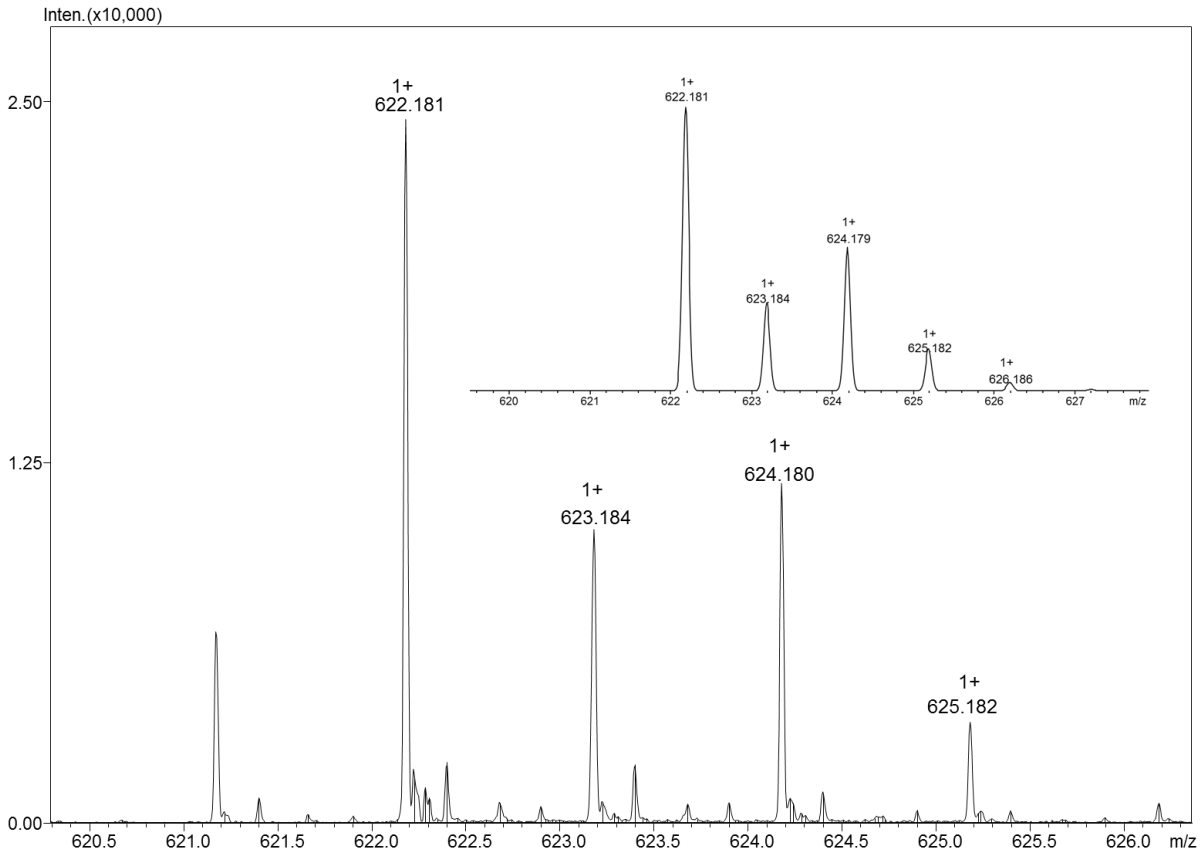

Figure S10a. ESI-MS spectrum of $[Cu(P1)H_{-1}]^+$ complex. Inlet presents the generated isotopic distribution for the $C_{26}H_{34}CuN_6O_8$ ion.

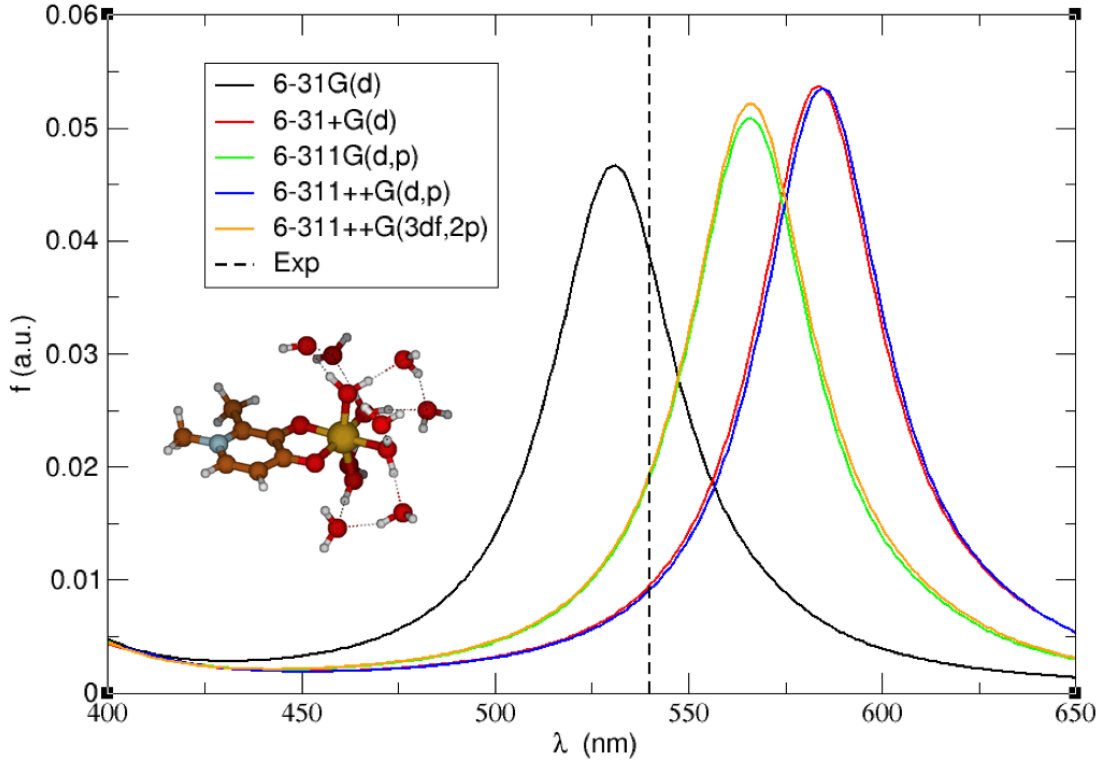

Figure S11. TDDFT spectra of Fe(DFP), using the WB97XD functional [D. Chai and M. Head-Gordon, "Long-range corrected hybrid density functionals with damped atom-atom dispersion corrections," Phys. Chem. Chem. Phys., 10 (2008) 6615-20. DOI: 10.1039/B810189B] and the SMD implicit solvation model [A. V. Marenich, C. J. Cramer, and D. G. Truhlar, "Universal solvation model based on solute electron density and a continuum model of the solvent defined by the bulk dielectric constant and atomic surface tensions," J. Phys. Chem. B, 113 (2009) 6378-96. DOI: 10.1021/jp810292n] with the addition of explicit second-shell water molecules.

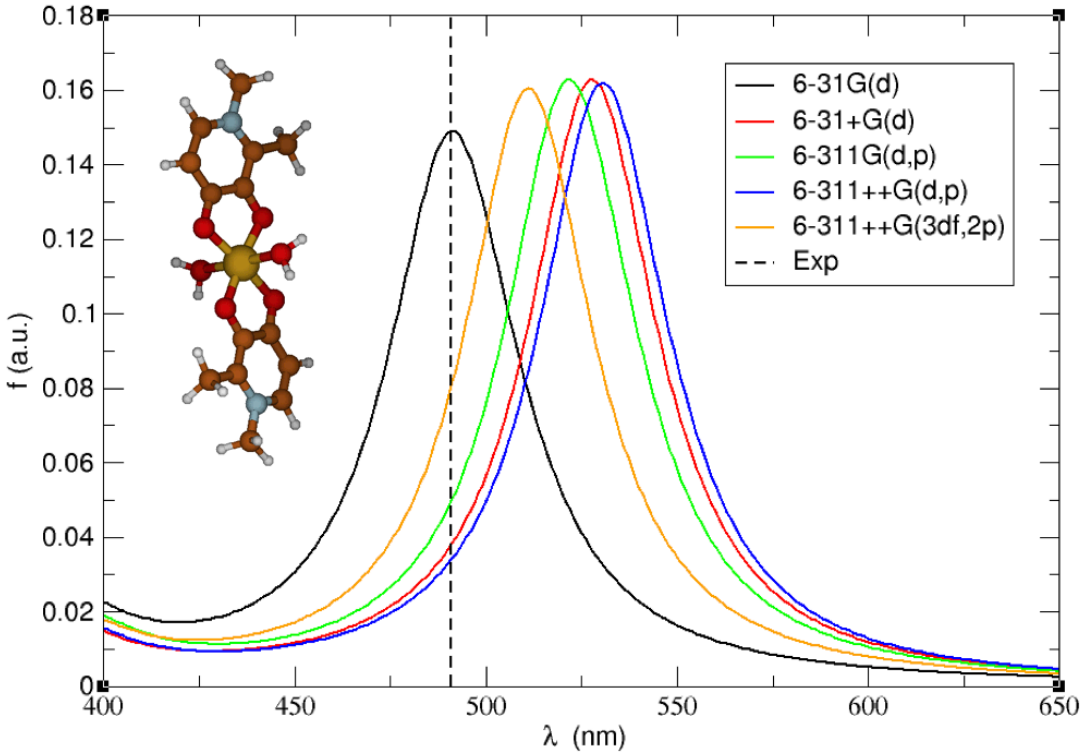

Figure S12. TDDFT spectra of $Fe(DFP)_2$, using the WB97XD functional [D. Chai and M. Head-Gordon, "Long-range corrected hybrid density functionals with damped atom-atom dispersion corrections," Phys. Chem. Chem. Phys., 10 (2008) 6615-20. DOI: 10.1039/B810189B] and the SMD implicit solvation model [A. V. Marenich, C. J. Cramer, and D. G. Truhlar, "Universal solvation model based on solute electron density and a continuum model of the solvent defined by the bulk dielectric constant and atomic surface tensions," J. Phys. Chem. B, 113 (2009) 6378-96. DOI: 10.1021/jp810292n].

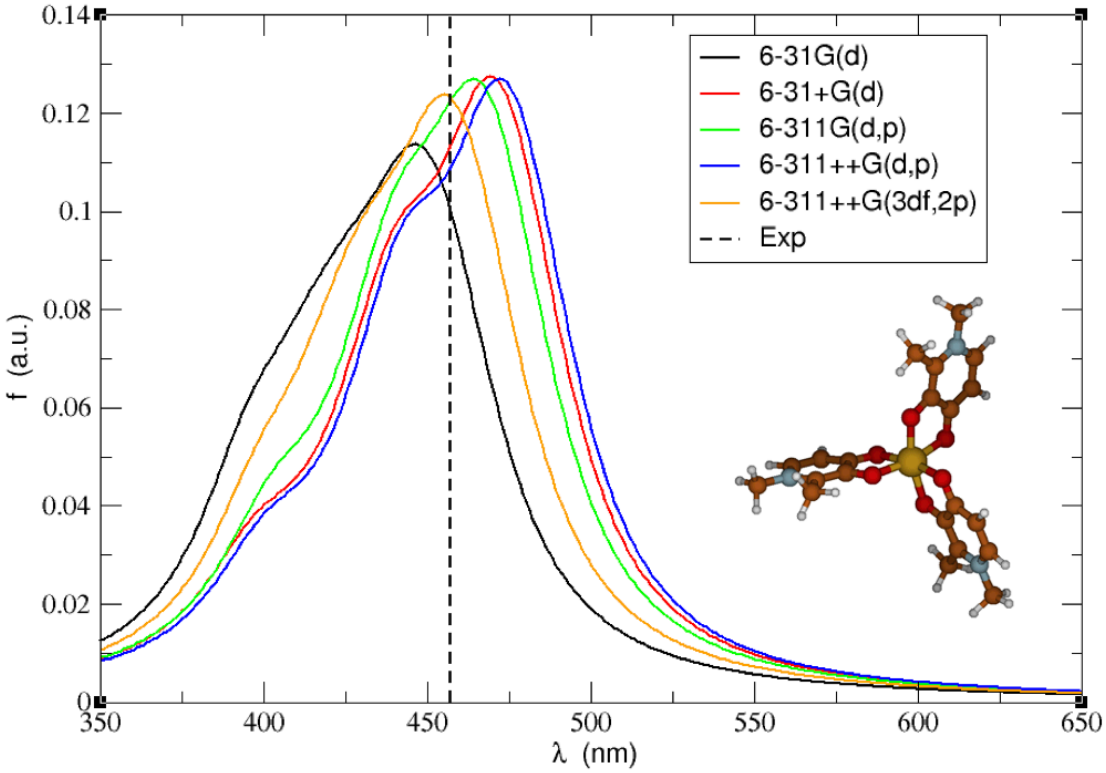

Figure S13. TDDFT spectra of $Fe(DFP)_3$, using the WB97XD functional [D. Chai and M. Head-Gordon, "Long-range corrected hybrid density functionals with damped atom-atom dispersion corrections," Phys. Chem. Chem. Phys., 10 (2008) 6615-20. DOI: 10.1039/B810189B] and the SMD implicit solvation model [A. V. Marenich, C. J. Cramer, and D. G. Truhlar, "Universal solvation model based on solute electron density and a continuum model of the solvent defined by the bulk dielectric constant and atomic surface tensions," J. Phys. Chem. B, 113 (2009) 6378-96. DOI: 10.1021/jp810292n].

In Figures S11 to S13, we can see the calculated TDDFT spectra for Fe(DFP), $Fe(DFP)_2$ and $Fe(DFP)_3$. We have chosen a long-range corrected functional such as WB97XD for these calculations using different basis sets. For Fe(DFP), we included a second shell of explicit waters to avoid spurious effects on the calculated spectra. Quite interestingly, the smallest of the basis sets used in this work, namely, 6-31G(d) provided the best agreement with the experiments, the inclusion of diffuse functions shifted the spectra to longer wavelengths, with a partial recover of the agreement with the experiments with the largest basis set, namely 6-311++G(3df,2p). In general, irrespective of the basis set, we observe the same behavior as in the experimental spectra: Fe(DFP) shows the lowest-energy absorption (higher wavelengths), followed by $Fe(DFP)_2$ and then $Fe(DFP)_3$.

Next, we calculated the spectra for Peptides 1 to 6 bound to Fe(III), using the 6-31G(d) and 6-311G(d,p) basis sets. Both basis sets gave the same qualitative results, depicted in Figures S4 and S5. Thus, Pept 1 to 3 show the absorption at the lowest energies (highest wavelengths) as Fe(DFP), in

correspondence with the situation found for Fe(DFP). On the other hand, Fe-Pept4 and Fe-Pept5 show absorption at intermediate regions, overlapping the absorption region of $Fe(DFP)_2$. Finally, Fe-Pept6 shows an absorption spectra similar to the one of $Fe(DFP)_3$, that is, at the lowest wavelengths (i.e., highest energies), in agreement with experiments, and suggesting a binding pattern to three mimosine sidechains similar to the coordination mode of $Fe(DFP)_3$.

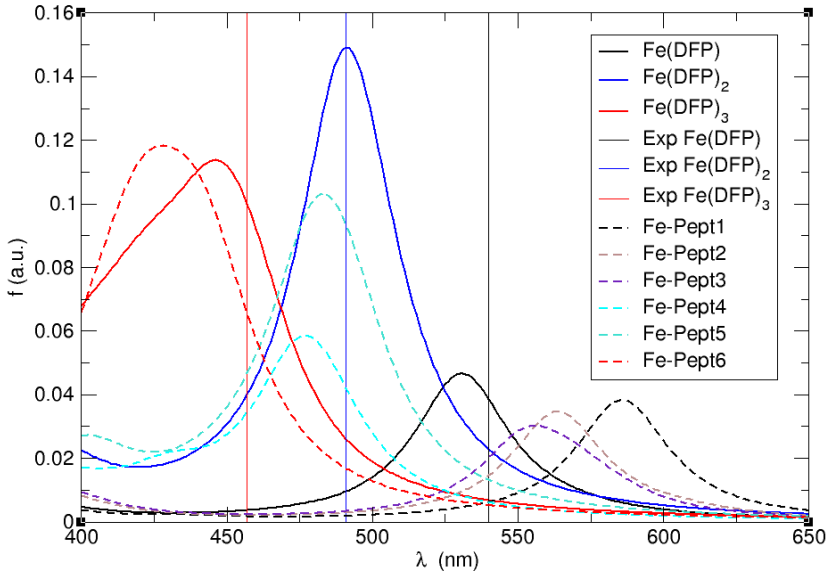

Figure S14. TDDFT spectra using the WB97XD/6-31G(d) functional [D. Chai and M. Head-Gordon, "Long-range corrected hybrid density functionals with damped atom-atom dispersion corrections," Phys. Chem. Chem. Phys., 10 (2008) 6615-20. DOI: 10.1039/B810189B] and the SMD implicit solvation model [A. V. Marenich, C. J. Cramer, and D. G. Truhlar, "Universal solvation model based on solute electron density and a continuum model of the solvent defined by the bulk dielectric constant and atomic surface tensions," J. Phys. Chem. B, 113 (2009) 6378-96. DOI: 10.1021/jp810292n], for the different peptides (peptides 1 to 6) bound to Fe(III), compared to the experimental and theoretical data for Fe(DFP), $Fe(DFP)_2$ and $Fe(DFP)_3$

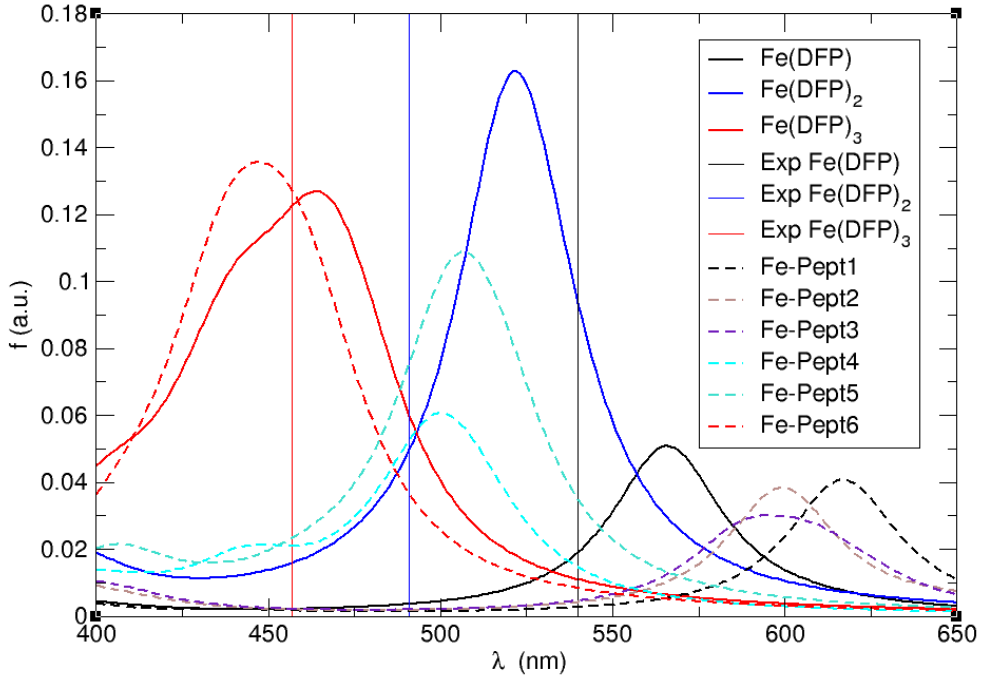

Figure S15. TDDFT spectra using the WB97XD/6-311G(d,p) functional[D. Chai and M. Head-Gordon, "Long-range corrected hybrid density functionals with damped atom-atom dispersion corrections," Phys. Chem. Chem. Phys., 10 (2008) 6615-20. DOI: 10.1039/B810189B] and the SMD implicit solvation model [A. V. Marenich, C. J. Cramer, and D. G. Truhlar, "Universal solvation model based on solute electron density and a continuum model of the solvent defined by the bulk dielectric constant and atomic surface tensions," J. Phys. Chem. B, 113 (2009) 6378-96. DOI: 10.1021/jp810292n], for the different peptides (peptides 1 to 6) bound to Fe(III), compared to the experimental and theoretical data for Fe(DFP), $Fe(DFP)_2$ and $Fe(DFP)_3$